

# A Deformable Model for Magnetic Vortex Pinning

J.A.J. Burgess<sup>1,2</sup>, J.E. Losby<sup>1,2</sup>, and M.R. Freeman<sup>1,2</sup>

<sup>1</sup> *Department of Physics, University of Alberta, Edmonton, Alberta, Canada T6G 2E1 and*

<sup>2</sup> *National Institute for Nanotechnology, Edmonton, Alberta, Canada T6G 2M9*

(Dated: August 21, 2012)

A model of the magnetic vortex in a thin disk of soft magnetic material is constructed. The model employs a piecewise merger of two of the most successful analytical models of the vortex state in a disk and is capable of describing the change in the characteristic warping of the magnetization distribution when the vortex core interacts with a magnetic pinning site. The constructed analytical model is compared to numerical simulations of ideal disks with and without pinning sites and is found to accurately predict the magnetization, vortex position, hysteretic transitions, and 2-D displacement of the vortex in the presence of pinning sites.

PACS numbers: 75.30.Hx, 75.60.Ch, 75.75.Fk

## I. INTRODUCTION

Interest in magnetic vortices<sup>1,2</sup> in thin disks has grown dramatically over the past two decades, as these are fundamental physical systems with direct applications to technology<sup>3</sup>. Topological structures such as vortices are stable, manipulable objects that show promise as logic elements or storage media in spintronics applications. The thin soft magnetic disk, the prototypical system containing a vortex, has therefore become an extensively investigated system. Properties studied include structure<sup>4,5</sup>, dynamical modes<sup>6-8</sup>, annihilation<sup>9,10</sup> and creation<sup>9,11-13</sup>. As each aspect of vortex physics is probed experimentally, and considered for technological applications, theoretical understanding via simulation and modeling is also advanced. Modeling is particularly important in the case of the thin ferromagnetic disk as it presents a well-defined system amenable to description by an analytical approach.

A recent focus of activity is the interaction of vortex cores or domain walls with film inhomogeneities. Physically, geometric defects or magnetic impurities can increase or decrease the energetic cost for the topological structure<sup>14</sup> creating preferential locations or altering the magnetization distribution. In the disk system, direct observations of vortex core pinning have been observed with Lorentz microscopy<sup>15</sup> while the effect on vortex gyration has been observed with time-resolved magneto-optical Kerr effect microscopy<sup>16-19</sup> and electronically<sup>20</sup>. Incorporation of pinning potentials into existing analytical models has permitted a qualitative description of the position of the vortex and its reduced displacement susceptibility<sup>21</sup>. This approach is insufficient for quantitative applications. Recent work using nanomechanical torque magnetometry has provided direct observation of the Barkhausen steps associated with jumps in core position<sup>22</sup>, necessitating the development of a model that permits a quantitative description of pinning effects. Physically one expects two clear contributions to the magnetic susceptibility of a pinned vortex, one from the magnetization distribution and one from rigid displacement of the vortex. An analytical model designed to

capture both contributions is presented here, and demonstrated to reproduce numerically simulated quasistatic vortex pinning behavior.

The vortex state ansatz was first developed for the magnetic disk by Aharoni in 1990<sup>23</sup>. Further work by Usov and Peschany<sup>4</sup> determined an exchange optimized functional form of the core magnetization profile. Good agreement between this model and simulation<sup>24</sup>, as well as experimental observation<sup>5</sup>, was found. This work considered the vortex ground state, at zero field. Subsequent work<sup>25,26</sup> considered the displacement of the core with field and annihilation field using a model that rigidly translated the magnetization distribution developed by Usov and Peschany. This is known as the Rigid Vortex Model (RVM). Recent extensions of the RVM include higher order versions developed to describe the susceptibility of the displaced vortex analytically<sup>10</sup>. Concurrently, more complex models approximating the flexing of the magnetization distribution were developed<sup>27,28</sup>. This class of model is equivalent to the influence on the magnetization distribution of a second vortex moving from infinity to the edge of the disk, and it is called the Two Vortex Model (TVM). Versions of this model have been applied to calculating the stability of the vortex state in a disk with moderate success<sup>27,28</sup> and, with greater success, to predict frequencies of dynamic modes<sup>29-31</sup>.

## II. CONSTRUCTION OF THE MODELS

Both the RVM and TVM link the computed model magnetization directly to the vortex core displacement in the disk using only a single parameter<sup>32</sup>. For each model the total energy is composed of the exchange, demagnetization, and external field energies as summarized below. Magnetocrystalline anisotropy is neglected.

### A. The Rigid Vortex Model

The RVM is derived by considering the vortex magnetization distribution ansatz<sup>4,23</sup> to be immutable and trans-

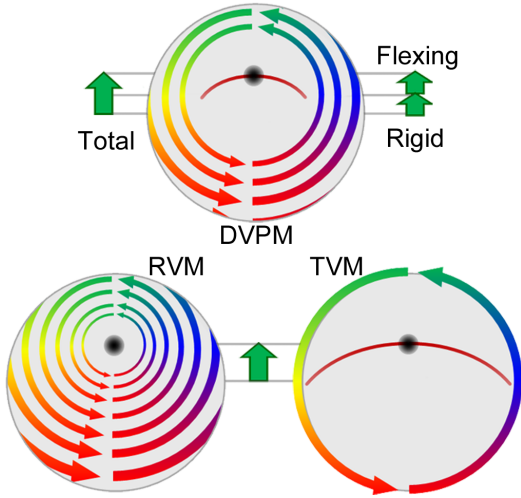


FIG. 1. (Color available in online version.) Schematics depicting the evolution of the magnetization distribution as the vortex core is displaced. The arrows, as well as the color scale, indicate the in-plane direction of the magnetization. At top is the DVPM which has two regions: an outer shell described by the RVM and an inner shell described by the TVM. Both components make contributions to the magnetization and vortex displacement allowing the DVPM to capture more complex behavior. By contrast the RVM (lower left) employs a parameter that governs both vortex and magnetization distribution displacement, while the TVM (lower right) has a single parameter that determines both magnetization distribution flexing and vortex displacement.

lating that distribution relative to the physical boundary of the disk (Figure 1). The normalized total energy for the 3rd order RVM<sup>10</sup> of a disk with a radius  $R$  and thickness  $L$  as a function of the reduced field  $h = H/M_S$  is given as

$$\frac{E_{tot}}{\mu_0 M_S^2 V} = \frac{\beta}{2} b^2 - h(b - \frac{b^3}{8}), \quad (1)$$

where  $b = \Delta r/R$  is the normalized core displacement,  $\beta = F_c(L, R) - R_o^2/R^2$  is a constant describing the demagnetization energy and exchange energy with  $F_c(L, R)$  representing the susceptibility-corrected demagnetization factor computed for the uniformly magnetized disk<sup>33</sup>, and  $R_o = \sqrt{2A/\mu_0 M_S^2}$  is the exchange length. The energy is normalized by  $\mu_0 M_S^2 V$  where  $V$  is the disk volume. It should be noted that the incorporation of the susceptibility correction to the demagnetization factor, the so called  $\mu^*$  correction<sup>34</sup>, is critical to the success of the model in application to a disk composed of a soft magnetic material (Figure 2 a, inset), but is often neglected. Solving the model permits calculation of the vortex displacement as a function of field,  $b_o(h) = (-4\beta + 2\sqrt{4\beta^2 + 6h^2})/3h$ , and consequently the magnetization  $m_o(h) = M_o(h)/M_S = b_o - b_o^3/8$ . Removing the third order term in the magnetization, and consequently the external field energy, reduces the model

to the second order RVM<sup>25,26</sup> with  $m_o(h) = b_o(h) = h/\beta$ .

## B. The Two Vortex Model

The TVM is derived by setting a boundary condition and computing the magnetization distribution that minimizes the exchange energy for a given vortex core displacement<sup>27,35</sup> (Figure 2b). Here the no side charges version of the model<sup>27,29</sup> is applied and the magnetization is held tangential to the disk edge. In the same form as used for the RVM, the total normalized energy may be written down for the TVM,

$$\frac{E_{tot}}{\mu_0 M_S^2 V} = \frac{\alpha}{2} a^2 - \xi h a, \quad (2)$$

where  $a/2 = \Delta r/R$  represents the normalized displacement,  $\alpha = RF_1(L, R)/L - R_o^2/2R^2$  incorporates the demagnetization energy and exchange energy, and  $\xi$  is a constant ( $\sim 10/29$ ). The function  $F_1(L, R)$  is an equivalent demagnetization factor describing the volume magnetostatic charges resulting from flexing of the magnetization distribution and is approximated as  $k(L/R)^2$  with  $k = 0.08827$ . As before, minimization with respect to  $a$  allows computation of  $a_o(h) = \xi h/\alpha$  and magnetization  $m_o(h) = \xi a_o(h)$ .

## C. The Deformable Vortex Pinning Model

In the RVM and TVM models, the direct dependence of the magnetization on the vortex displacement parameter means that, even in the presence of a local imperfection in an otherwise perfect disk, the core position and overall disk magnetization can not evolve independently. This implies, and numerical simulation confirms, a clear qualitative shortcoming of these models in the form of the flexing of the magnetization distribution evolution during pinning (See Supplementary Movies M1 and M2). A composite model, the Deformable Vortex Pinning Model (DVPM), can be constructed to correct this problem, incorporating both the RVM and TVM with two parameters.

The DVPM can be derived by dividing the disk into two regions, an outer annulus described by the RVM, and an inner disk of radius  $R_1$  described by the TVM with no side charges. The tangential boundary condition of the TVM maintains a piecewise continuity of the magnetization distribution between the two models. As field is applied, the center of the inner disk shifts along with the core position computed from the outer annulus. Concurrently, the computed core position in the inner region also deflects, deforming the central region magnetization. In this way, there are two contributions to vortex position as well as magnetization distribution. To self-consistently solve the two sections of

the model, it is necessary to consider the energetic components of each (Figure 2). Neglecting the susceptibility correction, derivation of the inner TVM energetic contributions would be independent of the outer annulus, and since the RVM contributions change only from the shift of the magnetization distribution relative to the boundary, the two models would be independent up to the point where the central region edge reaches the disk boundary. However, the susceptibility correction implicitly couples the two sections through the demagnetization energy. In the RVM, the susceptibility correction uses material susceptibility to estimate the net decrease of the demagnetization energy due to the reduction of side charges, and the introduction of volume charges parameterizing the real world magnetization flexing. But the TVM is already flexible, and therefore including the susceptibility correction for the shell, in addition to a central TVM region reduces the demagnetization cost of core deflection too much. This can be compensated for by increasing the energetic cost of deflection for the rigid shell a corresponding amount. This is equivalent to reducing the magnitude of the susceptibility correction. A linear interpolation between the corrected ( $F_c$ ) and uncorrected ( $F_{nc}$ ) demagnetization factors of the form  $F(L, R, R_1) = (1 - R_1/R)F_c(L, R) + (R_1/R)F_{nc}(L, R)$  is introduced. The equivalent change of the RVM shell demagnetization factor necessary to rebalance the energetic cost of vortex displacement is  $(R_1/R)^2(2R_1/L)F_1(R_1, L)$ . Comparing each, the deviation does not exceed 10% over the range  $R_1/R = 0$  to 1 for a linear interpolation, corroborating this interpretation<sup>36</sup>.

Using the interpolated demagnetization factor, the energy of the combined piecewise model may be written,

$$\frac{E_{tot}}{\mu_0 M_s^2 V} = \frac{\beta'}{2} b'^2 - h(b' - \frac{b'^3}{8}) + \gamma(\frac{\alpha'}{2} a'^2 - \xi h a'), \quad (3)$$

where  $\beta' = F(L, R, R_1) - R_o^2/R^2$  and  $\alpha' = R_1 F_1(L, R_1)/L - R_o^2/2R_1^2$ . Here  $b'$  is the normalized displacement of the outer RVM shell, and  $a'/2 = \Delta r_1/R_1$  is the central TVM core displacement normalized to  $R_1$ . The factor  $\gamma = R_1^2/R^2$  scales the energy contributions accordingly. All other symbols remain as before. The total core displacement is  $b' + R_1 a'/2R$  with the same expressions for  $b'_o(h)$  and  $a'_o(h)$  as before, but with  $\beta'$  and  $\alpha'$  replacing  $\beta$  and  $\alpha$  respectively. The corresponding magnetization is  $m_o(h) = b'_o(h) - b'_o(h)^3/8 + \gamma \xi a'_o(h)$ . For small displacements, the third order terms for the RVM shell may be dropped to make a simplified version of the model applicable for small displacements. For an ideal disk, the choice of  $R_1$  is not critical, the susceptibility correction interpolation mitigates variation with  $R_1$  for a wide range of disk aspect ratios. A value  $R_1 = R/2$  is used below.

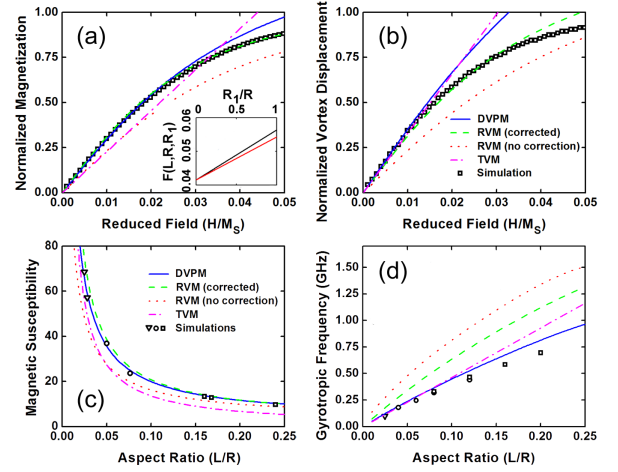


FIG. 2. (Color available in online version.) (a) The computed m-h curves from the four models discussed in this paper are compared against a simulation of a  $1\mu\text{m}$  diameter,  $30\text{ nm}$  thick disk with  $M_s=800\text{ kA/m}$ . (b) The computed vortex displacement as a function of field for each model is compared against the simulation. The legend inset in panel (b) applies to both (a) and (b). Only the RVM with a susceptibility-corrected demagnetization factor and the DVP describe both position and magnetization accurately for displacement  $< R/2$ . Inset in (a) is a comparison of the interpolation (solid red) used for the susceptibility correction applied in the DVP against the effective demagnetization factor required to balance the displacement contributions of the RVM and TVM regions in the DVP. This correction makes the computation insensitive with respect to variation of the size of the TVM region (radius  $R_1$ ). All DVP calculations in panels a-d use  $R_1 = R/2$ . (c) The computed initial susceptibility for all models is compared against simulation for disks of varying size. Simulations denoted with triangular point use a disk diameter of  $500\text{ nm}$ , circular points use  $1\mu\text{m}$ , and triangles use  $3.6\mu\text{m}$ . All simulations use  $M_s = 800\text{ kA/m}$  except the  $3.6\mu\text{m}$  which use  $M_s = 715\text{ kA/m}$ . (d) Using the same simulation parameters the mode frequency of the gyrotropic mode was computed. The legend in (c) applies to panel (d) as well. Only the DVP agrees well with both the initial susceptibility and the gyrotropic frequency. The corrected RVM correctly computes the susceptibility while the TVM closely estimates the gyrotropic frequency. For (c) and (d) calculations were performed holding  $R = 500\text{ nm}$  with variable thickness.

### III. APPLICATION TO THE IDEAL DISK

From Equations 1, 2, and 3 the ideal disk behaviour of each model may be computed and compared to Landau-Lifshitz-Gilbert micromagnetic simulation<sup>37</sup>. To mimic quasistatic behaviour, time integration with a damping factor of 1.0 was used. All simulations were performed on a 2-D  $5\text{ nm} \times 5\text{ nm} \times \text{thickness}$  grid using an exchange stiffness constant of  $1.05 \times 10^{-11}\text{ J/m}$ , with  $M_s$  values between  $700\text{ kA/m}$  and  $800\text{ kA/m}$  and either  $20\text{ nm}$  or  $40\text{ nm}$  thickness. All calculations with the model used an ex-

change length of 5.85 nm and  $M_S$  values matching the simulations.

Comparison of the  $m(h) = M(H/M_S)/(\mu_o M_S V)$  and  $r(h) = \Delta r(H/M_S)/R$  curves are shown in Figures 2 a and b. Clearly the susceptibility-corrected 3rd order RVM provides the best estimate of both magnetization and vortex displacement as a function of field, while the uncorrected version exhibits the poorest performance. Both the DVPM and TVM provide good estimates of vortex position with field for displacements up to  $R/2$ , but only the DVPM simultaneously gives a good description of the magnetization.

Two other metrics have been applied to evaluate the performance of the analytical models near zero field in past work: initial susceptibility, and the frequency of the lowest order excitation mode of gyrotropic vortex motion. Both of these parameters primarily depend on the aspect ratio of the disks. Initial susceptibility is easily calculated from  $m_o(h)$  for each model. Using the collective coordinate approach<sup>38</sup>, it may be shown that the gyrotropic mode frequency is  $f_o = \kappa/2\pi G$  where  $G = 2\pi L M_S/\gamma_o$  with  $\gamma_o = 1.76 \times 10^{11} \text{ s}^{-1} \text{ T}^{-1}$ , and  $dE_{tot}/dr = \kappa r$ <sup>29</sup>. For the RVM and TVM,  $\kappa$  is  $\beta$  and  $4\alpha$  respectively. For the piecewise combined model,  $\kappa$  may be computed in the unpinned and zero field case

$$\kappa = \frac{4(\alpha + \gamma \xi^2 \beta) \beta \alpha}{(2\alpha + \rho \xi \beta)^2}. \quad (4)$$

Dynamic simulations were performed using a realistic damping factor (0.02) but otherwise matched the parameters used in the previous simulations. The poor performances for magnetization description of the TVM and uncorrected RVM manifest as incorrect estimations of the initial susceptibility. However, both approach the simulation results for squat disks, corroborating previous results<sup>25,29</sup> and demonstrating the general utility of these models. By comparison, the DVPM and corrected RVM provide excellent estimates for all aspect ratios investigated. Previously, only the TVM has provided reasonable estimates for the gyrotropic frequency of the vortex state while the RVM has provided poor estimates. The success of the TVM is reproduced here, as is the failure of the uncorrected RVM. The susceptibility correction improves the RVM prediction, however it fails to match the performance of the TVM in the prediction of  $f_o$ . However, the DVPM provides comparable performance to the TVM for low aspect ratios and improved performance with more squat ideal disks.

#### IV. APPLICATION TO PINNING

Having demonstrated the performance of the piecewise model in a perfect disk, pinning may now be considered. Adding pinning to the models is accomplished by adding functions of the form  $E_p(b + R_1 a/2R - X_p)$  for a pinning site located at  $X_p$  to equation 3, or of the form  $E_p(b - X_p)$

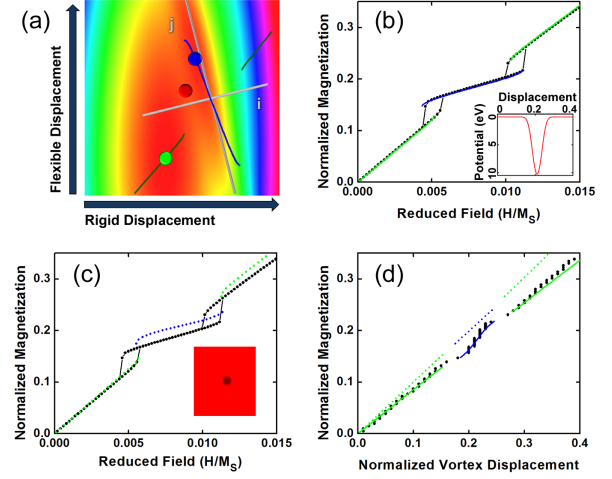


FIG. 3. (Color available in online version.) (a) The 2-D energy of the DVPM (color scale) is plotted as a function parameters  $b'$  (rigid) and  $a'$  (flexible) for a small applied field. A single pinning site is included, and the pinning site coordinate axes  $i$  and  $j$  are shown. At the applied field, local minima exist outside the pinning site (green disk at bottom) and inside the pinning site (blue disk at top) separated by an energy barrier lowest at a saddle point between the two minima (red disk in middle). The solid lines indicate the field evolution of the pinned and unpinned minima. Note that flexing evolves non-monotonically. (b) Solving for the minima as a function of field, and computing the corresponding magnetization yields an m-h curve that includes pinning effects (green and blue solid lines). The simulated results (black line with dots) for a  $1 \mu\text{m}$  diameter, 40 nm thick disk with a single large pinning site at 105 nm from the center. The pinning site is included in the model calculation at 107.5 nm with an energy profile estimated from the simulation (inset). The model m-h curves extend over the field range where a local minimum exists. (c) Incorporating pinning into the RVM (dotted blue and green lines) results in much larger positional error ( $> 10$  nm, shown uncorrected here) and a large underestimate of the hysteresis loop width. Inset is an image of the  $M_S$  suppression included in the simulation. The width of the pinning site is 40 nm, and at the center  $M_S = 550 \text{ kA/m}$ . (d) Plotting the simulated, and computed DVPM and RVM magnetization as a function of displacement shows that the DVPM accurately captures the change in the character of the displacement of the vortex during pinning as well as the contribution of flexing to the magnetization.

for the RVM in equation 1. For the RVM case, simply solving for the minima in energy permits a full solution of the problem. For the DVPM, the 2-D optimization required makes the problem more complicated, however this is critical to the success of the model. Plotting the pinning energy, pinning sites appear as linear troughs in a-b space (Figure 3 a). This permits a simplification of the optimization process by the consideration of pinning site coordinates defined by  $b = i \sin(\theta) + j \cos(\theta)$  and  $a = i \cos(\theta) - j \sin(\theta)$  for  $\theta = \tan^{-1}(2R/R_1)$ . Switching to  $i$  and  $j$  coordinates allows independent minimization



and simplifies the problem. Computation of the values of  $b$  and  $a$  to minimize the function permits description of the quasistatic pinned behaviour, while locating the saddle points separating minima allows computation of the energy barriers separating bistable states.

The critical feature of this minimization process is that the coordinate  $a$  may evolve non-monotonically with increasing field (Supplementary Material Movie M3) matching the qualitative non-monotonic evolution of the flexing of the magnetization distribution visible in simulation (Supplementary Movies M1 and M2).

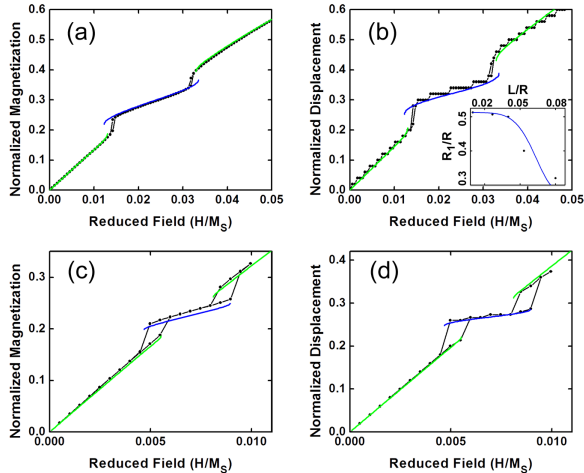


FIG. 4. (Color available in online version.) (a) The DVPM m-h result is compared to a simulation of a 500 nm diameter, 40 nm thick disk with  $M_S = 700$  kA/m and a single pinning site located 80 nm away from the center. (b) The computed displacements are compared for the same simulation. For this comparison  $R_1 = 80$  nm provides the best estimate of hysteresis loop width. The inset is a plot of the optimal  $R_1$  value found by comparison to simulation as a function of aspect ratio. The blue fit line is included as a guide to the eye. (c) Comparison to a simulated 1500 nm diameter, 40 nm thick disk with a single pinning site at 200 nm from center shows that the DVPM begins to underestimate the magnetization as disk size increases. (d) The computation of the vortex position and hysteresis loop width remains accurate. A  $R_1$  value of 375 nm was used.

Micromagnetic simulations were used to evaluate the pinning performance of the DVPM and, for comparison, the corrected RVM. The same simulation parameters were used as in the previous simulations. Pinning sites are mimicked using approximately circular regions of depressed saturation magnetization to modify the energy landscape of the disk (Figure 3 b inset). This leads to two contributions to pinning energy, the reduced exchange energy of the core in the low  $M_S$  region, as well as reduced demagnetization energy when the core is centered on the site. The energetic profile of the pinning site can be approximated by considering the convolution of a 2-D Gaussian at various offsets with the profile of the  $M_S$  variation (Fig 3b, inset). The Gaussian effectively ap-

proximates the exchange energy density of the core, as well as the  $M_z$  profile, providing an estimate of how the two energy contributions change as the core shifts relative to the pinning site. Here a full width half max of 17.2 nm is used for the exchange energy density.

The performance can be evaluated by three metrics, the pinning site position error, the width of the minor hysteresis loops associated with pinning and depinning, and the combined computed pinned differential magnetic and positional susceptibilities. Figure 3 b-d show results for a 1 micron diameter 40 nm thick disk compared to the DVPM and the 3rd order RVM. The DVPM accurately captures both differential susceptibilities while the RVM fails to capture the positional slope. Both models feature effective position shifts of the pinning site. The DVPM agrees best with the simulation for a pinning site shifted 2.5 nm further from center than the actual simulation, while a shift greater than 10 nm is best for the RVM. Most importantly, the computed entrance and exit hysteresis loops agree closely for the DVPM, but are almost non-existent for the RVM. The deformability of the DVPM permits the vortex to flex ahead into the site, and linger in the site at a lower energy cost than the rigid model.

Disk sizes between 500 nm diameter/40 nm thick and 2000 nm diameter/20 nm thick were simulated with identical  $M_S$  variation pinning sites. Unlike the perfect disk case, model performance for pinning is significantly affected by the choice of  $R_1$ . The amount of flexing permitted affects the vortex position and magnetization in the pinning site, and consequently, the energy barriers for entrance and exit from the pinning sites. The optimal  $R_1$  reflects the overall rigidity of the disk behavior. In general the value  $R_1 = R/2$  provides reasonable results. However for disks below 1  $\mu$ m in diameter (for 40 nm thickness) reduced  $R_1$  values provide better pinning performance (Figure 3d, inset) reflecting the increasing rigidity of smaller disks. The DVPM was found to give good estimates of hysteresis width and vortex position for all disk sizes when an optimized value of  $R_1$  was used. For disks significantly larger than 1  $\mu$ m in diameter, at 40 nm thickness, the pinned magnetic differential susceptibility was found to be underestimated, reflecting a change in the character of flexing in larger disk sizes. Figure 4 shows a 500 nm and 1500 nm diameter result for comparison.

### A. Two Dimensional Pinning Potentials

The DVPM provides excellent performance in the description of ideal disk behavior and pinning for idealized simulations. However, in application to real samples, the treatment of pinning sites located directly along the pathway followed by the vortex in the absence of pinning as it is deflected by field is limiting. As noted in recent numerical simulation work on pinning<sup>39</sup>, a more realistic case is to consider pinning sites near, but not centered on, the

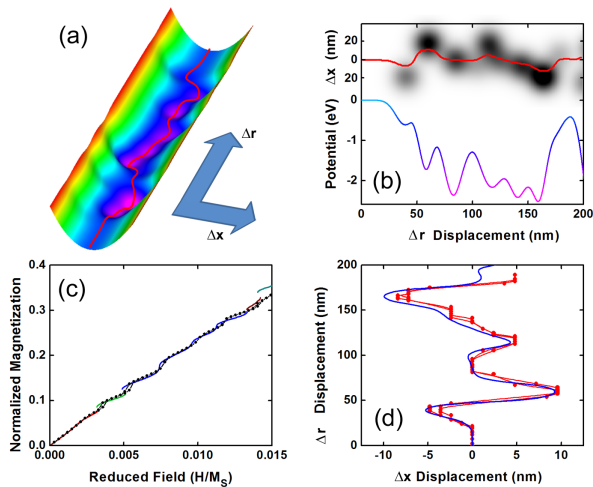


FIG. 5. (Color available in online version.) (a) A 3-D plot shows the combined pinning site potential and harmonic potential for deviations orthogonal to the path defined by the applied field. The computed path of minimum energy,  $\Delta x(\Delta r)$  is plotted as a red thread. (b) At top the 2-D pinning potential is plotted with the computed minimum energy path (red line). Below, the equivalent 1-D potential is presented. The equivalent potential incorporates contributions from both the pinning potential and harmonic trough. The color gradient on the line matches the color scale in panel (a). (c) The magnetization curve computed from the potential in (b) is compared against a simulated curve incorporating  $M_S$  suppressed regions with the same 2-D distribution. The depth of the 2-D potential used in the model calculations is estimated from the simulation. Agreement is close, though some deviations show up as the vortex displacement increases and a large energy change is encountered. (d) The simulated  $\Delta x(\Delta r)$  is compared to the computed minimum path showing excellent agreement.

field defined path. This can be incorporated into the 1-D model presented here by computing the 1-D equivalent potential of the actual 2-D path followed by the vortex. Deviations orthogonal to the path defined by the applied field have an energy cost approximated by  $\kappa \Delta x^2$  where the value of  $\kappa$  is given by equation 4. Since the magnetization induced by these deviations is orthogonal to the applied field, the energy is effectively static and can be summed with a 2-D distribution of pinning sites to form a trough guiding the vortex through the 2-D energy landscape. It is then possible to compute the minimum energy pathway  $\Delta x_o(\Delta r)$  that the vortex will follow as it is deflected (Figure 5a). Computing the total static energy, pinning plus the trough energy,  $E(\Delta x_o)$  yields an

equivalent 1-D potential as a function of  $\Delta r$  (Figure 5b). This potential can then be summed, as the Gaussian pinning sites were previously, with the potential for a perfect disk including field. Solving for minima as before allows computation of the evolution of the magnetization and vortex position in the 2-D potential.

This approach is applied to a simulation that incorporates a 2-D distribution of 10 nm diameter pinning sites with various values of suppressed  $M_S$  near the field defined path. As before, the pinning sites are incorporated into the model as Gaussian wells with depths estimated from the simulation and profiles computed by convolving a Gaussian with the profile of the  $M_S$  variation. The computed 2-D path agrees well with the vortex position extracted from simulation, as does the computed magnetization (Figure 2 c and d). Some disagreement is noted as the deflection increases close to the effective  $R/2$  limit of the model, and the vortex passes over a large barrier. In this computation, a sparse distribution of 2-D sites ensures a unique  $\Delta x_o(\Delta r)$ , however, in principle, this approach can be extended to bistable states in  $\Delta x$  by consideration of multiple vortex tracks. Computation of the energy barriers separating tracks, however, would require a more complete minimization.

## V. CONCLUSION

The piecewise approach applied to develop the DVPM yields a highly functional analytic model that makes quantitatively accurate predictions of a wide variety of properties of a vortex in a disk. Most notably it provides a powerful description of vortex pinning and provides greater physical insight into the behavior of the vortex during pinning. The model holds promise as a tool in probing the modification of pinning in technologically pertinent thin films to better understand effects such as ion damage, while the piecewise approach demonstrated may, in future, be generalized to other geometries, permitting quantitative computation of device behavior without cumbersome simulation.

## ACKNOWLEDGMENTS

We are grateful for support from the Natural Science and Engineering Council of Canada, the Informatics Circle of Research Excellence, the National Institute for Nanotechnology, the Canada Research Chairs program, and Alberta Innovates.

<sup>1</sup> R. P. Cowburn, D. K. Koltsov, A. O. Adeyeye, M. E. Welland, and D. M. Tricker, Physical Review Letters **83**, 1042 (1999).

<sup>2</sup> T. Shinjo, T. Okuno, R. Hassdorf, K. Shigeto, and T. Hono, Science **289**, 930 (2000).

<sup>3</sup> S. S. P. Parkin, M. Hayashi, and L. Thomas, Science **320**, 190 (2008).

- <sup>4</sup> N. A. Usov and S. E. Peschany, *Journal of Magnetism and Magnetic Materials* **118**, L290 (1993).
- <sup>5</sup> A. Wachowiak, J. Wiebe, M. Bode, O. Pietzsch, M. Morgenstern, and R. Wiesendanger, *Science* **298**, 577 (2002).
- <sup>6</sup> B. E. Argyle, E. Terrenzio, and J. C. Slonczewski, *Physical Review Letters* **53**, 190 (1984).
- <sup>7</sup> J. P. Park, P. Eames, D. M. Engebretson, J. Berezovsky, and P. A. Crowell, *Physical Review B* **67**, 020403 (2003).
- <sup>8</sup> S. B. Choe, Y. Acremann, A. Scholl, A. Bauer, A. Doran, J. Stöhr, and H. A. Padmore, *Science* **304**, 420 (2004).
- <sup>9</sup> V. Novosad, K. Y. Guslienko, H. Shima, Y. Otani, K. Fukamichi, N. Kikuchi, O. Kitakami, and Y. Shimada, *IEEE Transactions on Magnetics* **37**, 2088 (2001).
- <sup>10</sup> J. A. J. Burgess, D. C. Fortin, J. E. Losby, D. Grombacher, J. P. Davis, and M. R. Freeman, *Physical Review B* **82**, 144403 (2010).
- <sup>11</sup> J. P. Davis, D. Vick, J. A. J. Burgess, D. C. Fortin, P. Li, V. Sauer, W. K. Hiebert, and M. R. Freeman, *New Journal of Physics* **12**, 093033 (2010).
- <sup>12</sup> G. Mihajlovic, M. S. Patrick, J. E. Pearson, V. Novosad, S. D. Bader, M. Field, G. J. Sullivan, and A. Hoffmann, *Applied Physics Letters* **96**, 112501 (2010).
- <sup>13</sup> G. N. Kakazei, M. Ilyn, O. Chubykalo-Fesenko, J. Gonzalez, A. A. Serga, A. V. Chumak, P. A. Beck, B. Laegel, B. Hillebrands, and K. Y. Guslienko, *Applied Physics Letters* **99**, 052512 (2011).
- <sup>14</sup> D. Toscano, S. A. Leonel, R. A. Dias, P. Z. Coura, and B. V. Costa, *Journal of Applied Physics* **109**, 076104 (2011).
- <sup>15</sup> T. Uhlig, M. Rahm, C. Dietrich, R. Höllinger, M. Heumann, D. Weiss, and J. Zweck, *Physical Review Letters* **95**, 237205 (2005).
- <sup>16</sup> R. L. Compton and P. A. Crowell, *Physical Review Letters* **97**, 137202 (2006).
- <sup>17</sup> R. L. Compton, T. Y. Chen, and P. A. Crowell, *Physical Review B* **81**, 144412 (2010).
- <sup>18</sup> T. Y. Chen, A. T. Galkiewicz, and P. A. Crowell, *Physical Review B Rapid Communications* **85**, 180406 (2012).
- <sup>19</sup> T. Y. Chen, C. Erickson, M. J. and Leighton, and P. A. Crowell, (2012), arXiv:1201.1334.
- <sup>20</sup> J. S. Kim, O. Boule, S. Verstoep, L. Heyne, J. Rhenius, M. Kläui, L. J. Heyderman, F. Kronast, R. Mattheis, C. Ulysse, and G. Faini, *Physical Review B* **82**, 104427 (2010).
- <sup>21</sup> F. A. Apolonio, W. A. Moura-Melo, F. P. Crisafuli, A. R. Pereira, and R. L. Silva, *Journal of Applied Physics* **106**, 084320 (2009).
- <sup>22</sup> J. A. J. Burgess, A. E. Fraser, et al., To Be Published (2012).
- <sup>23</sup> A. Aharoni, *Journal of Applied Physics* **68**, 2892 (1990).
- <sup>24</sup> W. Scholz, K. Y. Guslienko, V. Novosad, D. Suess, T. Schrefl, R. W. Chantrell, and J. Fidler, *Journal of Magnetism and Magnetic Materials* **266**, 155 (2003).
- <sup>25</sup> K. Y. Guslienko, V. Novosad, Y. Otani, H. Shima, and K. Fukamichi, *Physical Review B* **65**, 024414 (2001).
- <sup>26</sup> K. Y. Guslienko, V. Novosad, Y. Otani, H. Shima, and K. Fukamichi, *Applied Physics Letters* **78**, 3848 (2001).
- <sup>27</sup> K. L. Metlov and K. Y. Guslienko, *Journal of Magnetism and Magnetic Materials* **242**, 1015 (2002).
- <sup>28</sup> K. Y. Guslienko and K. L. Metlov, *Physical Review B Rapid Communications* **63**, 100403 (R) (2001).
- <sup>29</sup> K. Y. Guslienko, B. A. Ivanov, V. Novosad, Y. Otani, H. Shima, and K. Fukamichi, *Journal of Applied Physics* **91**, 8037 (2002).
- <sup>30</sup> K. S. Buchanan, M. Grimsditch, F. Y. Fradin, S. D. Bader, and V. Novosad, *Physical Review Letters* **99**, 267201 (2007).
- <sup>31</sup> K. Y. Guslienko, R. H. Heredero, and O. Chubykalo-Fesenko, *Physical Review B* **82**, 014402 (2010).
- <sup>32</sup> The TVM uses a second parameter to describe distortions of the core profile under deflection, however this does not have a significant influence on the overall disk magnetization as a function of vortex displacement.
- <sup>33</sup> D. X. Chen, E. Pardo, and A. Sanchez, *Journal of Magnetism and Magnetic Materials* **306**, 135 (2006).
- <sup>34</sup> C. S., *Physics of Ferromagnetism*, 2nd ed. (Oxford University Press, 1997).
- <sup>35</sup> K. L. Metlov, *Physical Review Letters* **105**, 107201 (2010).
- <sup>36</sup> Here interpolation is chosen over the estimated rebalancing energy to maintain the limiting values at the susceptibility-corrected demagnetization factor and the uncorrected value.
- <sup>37</sup> All simulations were performed using version 2.56d of the LLG Micromagnetics software package <http://llgmicro.home.mindspring.com/>.
- <sup>38</sup> A. A. Thiele, *Physical Review Letters* **30**, 230 (1973).
- <sup>39</sup> G. M. Wysin, *Journal of Physics:Condensed Matter* **22**, 376002 (2010).

## VI. SUPPLEMENTARY MATERIAL: A DEFORMABLE MODEL FOR MAGNETIC VORTEX PINNING

The first movie (M1) shows the magnetization distribution of the disk from the simulation that generated the data used in Figure 3 in the main text. The magnetization direction is indicated by the color. Red indicates magnetization in the positive  $x$  direction, green is negative  $x$ , blue is positive  $y$  and yellow is negative  $y$ .

As the vortex is displaced by the field, the magnetization distribution warps away from the circularly symmetric initial vortex state. As the vortex interacts with the pinning site, the warping changes, and the flexing of the distribution decreases. This results from the continued biasing of the magnetization distribution outside of the core effectively mimicking continued displacement of the outer region while the core has reduced mobility. This can be challenging to see on the color scale. A second movie (M2) of the same simulation shows only the  $x$  component of the magnetization in a contour plot. The non-monotonic evolution of the contours stands out more clearly.

The third movie (M3) shows the evolution of the energy (color scale) of the vortex for a given location dependent on the parameters  $a'$  and  $b'$  computed in the model as magnetic field increases. The vertical axis is  $a'$  and  $b'$  is the horizontal coordinate. The single pinning site shows up as a trough across  $a', b'$  space. As the field increases, the unpinned vortex position (blue dot) increases and a second minimum appears in the pinning trough (red dot). As the field increases further, the vortex position outside the pinning site continues to increase in both  $a'$  and  $b'$ , but the pinned minimum decreases in  $a'$ . This effectively captures the behavior in the simulated movie. The flexing decreases, while the outer region continues to displace.

In addition to providing the opportunity to determine the positions of energetic minima to compute the unpinned and pinned magnetization and vortex displacement curve as a function of field, the saddle point separating the two minima may also be computed, allowing calculation of the energetic barrier separating the two.